

# JGR Space Physics

## RESEARCH ARTICLE

10.1029/2024JA033390

## Pick-Up ion Distributions in the Inner and Middle Saturnian Magnetosphere



### Key Points:

- pitch angle (PA) distributions of pick-up ions (PUIs) are overwhelmingly of the “pancake” type and widen with increasing latitude
- The PA distribution widths are inversely correlated with the amplitude of ion cyclotron waves (ICWs) in the same region
- Velocity distributions are generally constant throughout the extended neutral cloud, up to the orbit of Rhea where they begin to broaden

### Correspondence to:

C. R. Radulescu,  
[cristian.radulescu.17@ucl.ac.uk](mailto:cristian.radulescu.17@ucl.ac.uk)

### Citation:

Radulescu, C. R., Coates, A. J., Simon, S., Verscharen, D., & Jones, G. H. (2025). Pick-Up ion distributions in the inner and middle saturnian magnetosphere. *Journal of Geophysical Research: Space Physics*, 130, e2024JA033390. <https://doi.org/10.1029/2024JA033390>

Received 7 OCT 2024

Accepted 8 JAN 2025

### Author Contributions:

**Formal analysis:** Cristian R. Radulescu, Daniel Verscharen

**Supervision:** Andrew J. Coates, Sven Simon, Daniel Verscharen, Geraint H. Jones

**Writing – review & editing:** Cristian R. Radulescu, Sven Simon

Cristian R. Radulescu<sup>1,2</sup> , Andrew J. Coates<sup>1,2</sup> , Sven Simon<sup>3</sup> , Daniel Verscharen<sup>1</sup> , and Geraint H. Jones<sup>4</sup> 

<sup>1</sup>Mullard Space Science Laboratory, UCL, Surrey, UK, <sup>2</sup>Centre for Planetary Science at UCL/Birkbeck, London, UK, <sup>3</sup>Georgia Institute of Technology, Atlanta, GA, USA, <sup>4</sup>European Space Research and Technology Centre, Noordwijk, The Netherlands

**Abstract** Based on the entire dataset collected by the Cassini Plasma Spectrometer, we provide a comprehensive picture of the pitch angle (PA) and velocity distributions of pick-up ions (PUIs) in Saturn's inner and middle magnetosphere. We investigate the dependence of these distributions on Saturnian Local Time and magnetic latitude. We also search for correlations with the signatures of ion cyclotron waves (ICWs) observed by the Cassini magnetometer. Our survey reveals that ion PA distributions have a pancake shape and their full width increases monotonically with magnetic latitude. This increase in angular width is anti-correlated with the observed amplitudes of ICWs that are generated during the thermalization of the PUI distribution. We find no evidence of the previously observed, non-monotonic change of wave amplitudes with magnetic latitude mapping into the width of the PA distributions. This suggests that only a small fraction of the energy deposited into the waves is transferred back to the ions to broaden the distribution. We find that the PA scattering time is several times the bounce period, meaning PUIs become PA scattered only after completing several cycles of bounce motion and, hence migrating to higher latitudes by the time they become more isotropic. When moving away from Saturn's magnetic equatorial plane, the observed half-width of the velocity distributions does not evolve appreciably with latitude and  $L$  shell value. This behavior changes only outside the orbit of Rhea where the observed velocity distributions begin to broaden due to elevated plasma temperatures.

## 1. Introduction

Pick-up ions are charged particles that have been accelerated by electric and magnetic fields beyond the speed of the bulk plasma and then proceed to thermalize through wave-particle interactions. These types of particles have been observed at rocky planets (Brace et al., 1987; Keckskemety & Cravens, 1993), gas giants (Sittler et al., 2000), solar system moons such as Rhea (Desai et al., 2018; Teolis et al., 2010), Dione (Nordheim et al., 2020; Tokar et al., 2012), and Earth's moon (Mall et al., 1998; Poppe et al., 2016), as well as comets (Coates et al., 1989, 1993; Coates, Johnstone, et al., 1990; Gloeckler et al., 1986; Johnstone, 1995) and in the interplanetary medium (Kallenbach et al., 2000). The pick-up process (Coates, 2010, 2012, 2017) starts with neutral atoms and molecules that are ionized, via photoionization, charge exchange or electron impacts, turning them into charged particles. The newly created ions can be accelerated (“picked up”) by the electric and magnetic fields, up to twice the bulk plasma speed in the perpendicular direction to the magnetic field direction, which corresponds to the solar wind velocity for comets and corotation velocity for planets. From there the newly picked-up ions start gyrating due to  $E \times B$  drift and may develop a non-gyrotropic distribution while within distances of  $\sim 2$  gyroradii from the point of injection. After at least a full gyration the particles start describing a ring in velocity space, or cycloid in real space. This ring distribution is unstable, and wave particle interactions lead to PA scattering. The result of this scattering is a broadening of the ring distribution into, initially, a spherical shell centered on the bulk plasma velocity. As particles exchange energy with the waves, they will diffuse on paths in velocity space where they would conserve energy with the waves. These paths describe two shells centered on the phase velocities of the waves parallel and antiparallel to the magnetic field and hence create a bispherical shell distribution (Coates, Wilken, et al., 1990). The ions can continue to interact and exchange energy with waves which results in the ions being accelerated further until a drifting Maxwellian distribution is reached.

In this paper, we investigate specifically PUIs in the Saturn system. Here, the primary source of PUIs is the moon Enceladus. Located at  $\sim 3.9R_S$  (Radius of Saturn:  $R_S = 60268$  km), its southern hemisphere plumes eject large amounts of water into the Saturnian magnetosphere (Dougherty et al., 2006; Porco et al., 2006; Tokar et al., 2006).

©2025. The Author(s).

This is an open access article under the terms of the [Creative Commons Attribution License](https://creativecommons.org/licenses/by/4.0/), which permits use, distribution and reproduction in any medium, provided the original work is properly cited.

The ejected material creates the neutral torus where ionization mechanisms create ions which then interact with the electric and magnetic fields becoming PUIs. The plasma environment has previously been investigated on a global scale by Thomsen et al. (2010), who calculated the plasma moments (density, temperature and pressure) and composition for the bulk plasma at radial distances up to  $30R_S$ , with an emphasis on the region within  $17R_S$ . This investigation found that water group ions (hereafter  $W^+$ ) are mostly confined to the region near the equator due to their high mass, and dominate only up to  $3R_S$  above and below the equator. It was also found that within  $10R_S$  the plasma temperature increases sharply with radial distance. This behavior is attributed to PUIs that are injected at velocities close to corotation and then later thermalize by transferring their energy to the plasma through collisions and wave-particle interactions. However, in the study by Thomsen et al. (2010), the Maxwellian background (core) population was not separated from the PUI population which is initially highly anisotropic and more energetic than the already thermalized core. This population comprises the bulk of the plasma in Saturn's magnetosphere and is comprised of thermalized ions that are distributed isotropically. Thomsen et al. (2010) found that the ion temperature increases with  $L$  shell suggesting PUIs are likely the primary contributor to the ion energy. However, the exact distribution in density cannot be distinguished as new PUIs make up only a small fraction of the overall ion density. Additionally, Thomsen et al. (2010) focused their study on the equatorial region and so changes in the distributions with latitude were not investigated. A dedicated PUI survey at both the equator and high latitudes that removes the influence of the Maxwellian core is needed to better determine the distribution and properties of the PUIs.

Previous investigations of the distribution of PUIs have addressed the regions near Saturn's icy moons (Desai et al., 2017; Hartle et al., 2006; Regoli et al., 2016; Sittler et al., 2004; Teolis et al., 2010; Tokar et al., 2008). They determined the density, composition, PA and velocity distribution of PUIs only in the regions immediately downstream of the moons and their exospheres. As previously mentioned, the material ejected by the Enceladus plumes creates a neutral torus around Saturn. The water molecules ejected by the Enceladus plumes initially create a torus close to the orbit of Enceladus. These  $H_2O$  molecules then proceed to photodissociate into OH molecules over a period of 2.5 months creating an extended torus. Over a further 1.3 hr, photodissociation leads to the creation of an even more extended oxygen torus extending up to the orbit of Titan (Smith et al., 2010). Of the neutrals making up the tori, only a small percentage (up to 26%) get ionized with the rest being tied up in processes such as charge exchange and collisions (Cassidy & Johnson, 2010; Fleshman et al., 2010). Most of this ionization occurs in the torus itself, rather than around the moons (Cassidy & Johnson, 2010; Jurac & Richardson, 2005). Inside radial distances up to  $8R_S$  most of the ions have their origin at local sources rather than from radial transport from deeper in the magnetosphere (Bagenal & Delamere, 2011). In the area around Enceladus electron impact is more efficient and hence dominates over other ionization processes, resulting in less efficient ionization. However electron impact becomes less important as we move away from Saturn until we reach around  $7-9R_S$  where photoionization dominates (Sittler et al., 2008; Y. Chen et al., 2010; Cassidy & Johnson, 2010). It can be safe to assume that PUIs can be found in abundance within  $9R_S$  and likely beyond.

For this reason, we aim to gain a better understanding of the distribution of PUIs at Saturn by performing a global investigation of the PA, velocity and density distribution of these ions. Global studies of the occurrence and distribution of plasma waves and other particles have also been performed. Leisner et al. (2006) carried out the first ICW studies after the arrival of Cassini at Saturn finding clear evidence of ICWs at the gyrofrequency of water group ions ( $O^+$ ,  $OH^+$ ,  $H_2O^+$ ,  $H_3O^+$ ). Leisner et al. (2011) furthered the search for ICWs at higher latitudes and discovered that ICWs peaked in amplitude at around  $0.2R_S$  north and south of the equatorial plane rather than exactly at the equator where a local minimum was present. In the data this manifested as an "M" when amplitude is plotted with respect to latitude at a given radial distance. We will henceforth refer to this feature as the M-like signature. These findings are further confirmed by later studies that used magnetometer data from the entire Cassini mission (Chou & Cheng, 2017; Long et al., 2022; Meeks et al., 2016; Meeks & Simon, 2017). We will compare our findings to these previous results in order to determine if observations such as the Leisner et al. (2011) M-like signature can be observed in the PUI distributions. This will also give us a better understanding of how ICWs are produced as well as what other effects ICWs can have (e.g., their potential influence on MeV electron distributions through wave particle interactions (Santolik et al., 2011)).

This paper is broken down into six sections. In Section 2 we describe the data used for this study and the instrument that obtained this data. In Section 3 we go through the methods used in analyzing the PA distributions

(PADs). In Section 4 we present the final distribution maps. In Section 5 is a discussion of the results. Finally, in Section 6 we summarize this project and present the final conclusions.

## 2. Data and Instrumentation

In this study, we use data from the Cassini Plasma Spectrometer (CAPS) (Young et al., 2004) and magnetometer (Dougherty et al., 2004) on board the Cassini spacecraft. The CAPS instrument was a plasma spectrometer and comprised three sensors that measured the different thermal components of the plasma: the Electron Spectrometer (ELS), Ion Mass Spectrometer (IMS) and an Ion Beam Spectrometer (IBS). Of these, only the first two are used in this paper. ELS was a hemispherical top hat electrostatic analyzer (ESA) that separated electrons by energy per charge with a range of 0.6–28,750 eV/e and an energy resolution  $(\Delta E/E)_{FWHM}$  of 0.17. The analyzer included 8 anodes with an angular resolution of  $5.2 \times 20^\circ$  and a time resolution of 2 s. IMS consisted of a combination of a toroidal ESA with a carbon-foil time-of-flight (TOF) mass spectrometer. The ESA provided a measurement of the ion energy per charge, with a range of 1–50,280 eV/e, resolution of 0.17 and time resolution of 4 s (32 s per A cycle), while TOF measured the velocity, and hence the mass per charge of the particles, allowing the identification of different species in the measured plasma. It included 8 anodes, each with an angular resolution of  $8.3 \times 20^\circ$ . The Cassini magnetometer (MAG) consisted of a flux gate magnetometer (FGM) with a sampling rate of 64 vectors/s and a vector helium magnetometer (V/SHM) with a sampling rate one sixteenth that of the FGM. These measured small fluctuations in the magnetic field, permitting the accurate determination of plasma waves and other processes that influence the magnetic field. The CAPS instrument was also mounted on an actuator that scans  $-80^\circ$  to  $104^\circ$  in the planer direction, giving the instrument a wider field of view.

The Cassini spacecraft orbited around Saturn from 2004 to 2017, however the CAPS instrument was finally turned off in 2012 due to spacecraft safety concerns and hence this study uses a data set from 2005 to 2012. The year 2004 was omitted from our data set due to the data in the early days of the mission being predominantly too deep in the magnetosphere, with many maneuvers and different operation modes that make it harder to compare to data from later years. Information about electron number density calculated using data from CAPS-ELS, while PA, density and energy are taken from the CAPS-IMS data. The Cassini magnetometer provides us with information on the strength and orientation of the magnetic field.

## 3. Distribution Processing

The bulk of  $W^+$  ion density can be found in the inner magnetosphere ( $R < 6R_S$ ), extending slightly into the middle magnetosphere ( $6R_S < R < 15R_S$ ) (Arridge et al., 2011), with number density ratios between heavy ions and protons dropping below 50% past  $8R_S$  (Thomsen et al., 2010; Wilson et al., 2008; Young et al., 2005). The highest ion production efficiency is in the range of 7–9  $R_S$  (Smith et al., 2010). Meeks and Simon (2017) also did not detect any ICWs past  $8.1 R_S$ . Hence, for this study we limit our analysis to dates when Cassini was within 10  $R_S$  from the center of Saturn, a region that approximately corresponds to the extended neutral cloud (Johnson et al., 2006; Sittler et al., 2008; Smith et al., 2010; Y. Chen et al., 2010; Cassidy & Johnson, 2010), as this allows us to examine the areas with highest water group ion density and ICW occurrence as well as including the orbit of Rhea. The Cassini spacecraft spent varying amounts of time in this region, with the bulk of its time being spent in the outer magnetosphere due to its velocity being much lower in this region. Hence, for this study we isolate the dates during which Cassini passed through our region of interest. We perform this study for the entire period in which CAPS was functional with most years having on average 30 days that could be used for data retrieval. Figure 1 shows the orbit segments used for this study.

ELS, IMS and MAG have different sampling rates that also changed throughout the mission depending on the mode used. We exclude some of the measurements in order to make the correct correspondence between data sets of various instruments. The data sets are synchronised using the counting rate from the instrument with the lowest one, usually IMS, in order to avoid the creating of new points through interpolation required to fill the gap left by the lower counting rate or alternatively averaging over different counting rates. We then compare IMS time stamps to time stamps of the data obtained from the other instruments. The data point closest to each IMS timestamp is kept and the rest are excluded from our analysis. The reduced MAG data set was used only sparingly for the calculation of the cyclotron frequencies. We also do not expect the magnetic field to vary significantly over

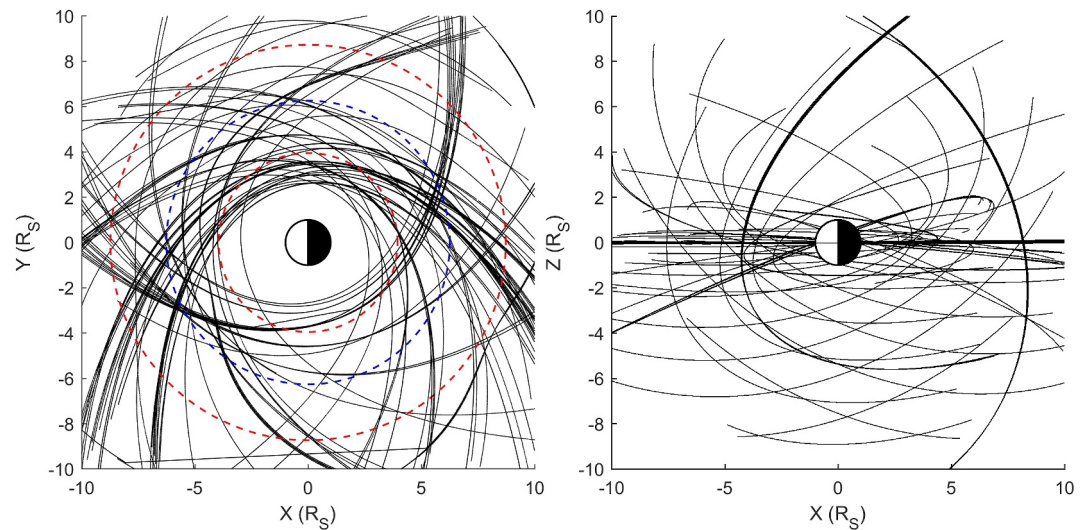


**Figure 1.** Top-down view (left) and side view (right) of the Saturn system in Kronocentric Solar Magnetospheric Coordinates (KSM) with the  $X$  axis being on the Saturn-Sun line (Sun on the left-hand side of the figure), the  $Z$  axis being parallel to the planet's rotation axis and the  $Y$  axis completes the right handed coordinate system. The orbit segments used for analysis are shown as black curves. The dotted lines show the orbits of (in order of increasing distance from Saturn): Enceladus, Dione and Rhea ( $4R_S$ ,  $6.2R_S$  and  $8.7R_S$  respectively).

the measured period and so we expect this method to not have detrimental effects on our analysis beyond a slight reduction in accuracy.

For each identified date, we split the data into 10 min intervals. We chose this interval in accordance with the technique used by Meeks et al. (2016). They argued this to be an adequate interval for studying ICWs due to it being one order of magnitude larger than the expected ion cyclotron period while also being shorter than the time needed for Cassini to move a distance on the order of  $1R_S$ . The observed breaks in the ion counts is a result of the actuator moving the CAPS field-of-view, with the peaks being times during which the instrument was looking into the direction of corotation. One of the notable features is the presence of a significant background in the region close to Saturn, a result of penetrating radiation, making ion signatures hard to resolve. We remove this background by taking the 3 highest energy bins that contain data, averaging them and subtracting this value from the counts data, doing this for each time step individually. An example of Cassini CAPS data and a comparison between data with and without the background radiation included is presented in Figure 2.

Following the approach of Tokar et al. (2008), we check for the presence of PUIs by subtracting the bulk population counts from the ion data. Figure 3 shows a slice through the ion counts data. This subtraction is only done within areas where CAPS was looking into the corotation direction (i.e., the high count rate areas). After experimenting with several values, we set a lower limit for this subtraction to  $5 \times 10^3$  counts/s for the equatorial region, decreasing at higher latitudes in accordance to scale height (Bagenal & Delamere, 2011). This specific value was chosen as it was found to remove cases that could not be adequately fitted, while minimizing the exclusion of good cases. We used a least squares fit method to fit a Maxwellian distribution to the counts data, making sure the peak of the distribution matches the peak in the data. The simulated counting rate is subtracted from the measured counts up to the expected maximum energy of PUIs. In the CAPS frame of reference, the measured maximum velocity of freshly created PUIs is  $v = 2v_{co} - v_{sc}$ , where  $v_{co}$  is the (sub)corotation velocity and  $v_{sc}$  is the spacecraft velocity. This is a slightly different approach to that used by Tokar et al. (2008). We vary the reference bulk velocity within the range of values presented by Wilson et al. (2009) leading to changes in the goodness of the fits, however our conclusion is not affected by these variations. In some of the time slices, the Maxwellian fit passes through or even above the measured data points, even past the expected PUI energy (vertical line in Figure 3). In this case, the core and PUI distributions are harder to separate from each other. When omitted from the analysis, the results are unaffected, meaning there are comparatively few of these cases and we decided to keep them in the analysis for completeness.

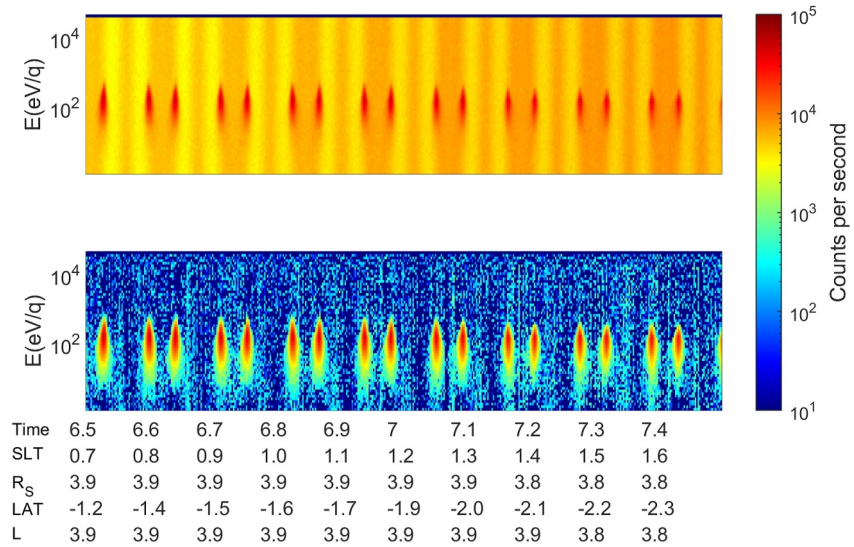


**Figure 2.** An example of Cassini CAPS-IMS Singles (SNG) (anode 4) data from 24 October 2007 (top). It also shows the data for the same time interval after the background radiation has been removed (bottom). SLT refers to Saturn local time, LAT to the spacecraft latitude, and L the local L-shell.

In order to understand how PUIs are distributed in PA and velocity, we plot their phase space density (PSD) as a function of velocity and PA. We obtain PA information from the 8 anodes of IMS. Each 20° anode's look direction gives us the direction of the velocity of incoming ions, while the magnetometer gives us the direction of the magnetic field. The PA is then calculated as the dot product between the flow direction (opposite of the look direction) and the magnetic field. An average PA is calculated for each anode from values computed for each of the four corners of the anode. Each anode detects ions using 63 energy bins, with each bin having a central value and covering ions with energies 8.5% above and below that value. We limit the ion energy to between 90 eV and 1.7 keV, which is the energy range specific for water group ions in the region around Enceladus (Tokar et al., 2008).

We also shift this energy window upwards with increasing radial distance because of the bulk plasma velocity increasing the energy of ions as we move away from Saturn. Since water group ions have masses that range from 16 for  $O^+$  to 19 for  $H_3O^+$ , we use a mass of 16.25 for our calculations, which is between that of  $O^+$  and  $OH^+$ , the most common water group ions. Wilson et al. (2008, 2009) found that the plasma is sub-corotating at distances further than  $3R_s$ , and so we use the fit from Wilson et al. (2008) for our azimuthal velocity profile. Knowing this, we then calculate the ion velocities from the measured energies and from there obtain the injection velocity  $v_{inj}$ . The data are plotted using a fan-shaped grid with 3 km/s by 5.7° radial bins. Since each anode has a width of 20° and each energy bin covers a finite range, we evenly distribute the calculated PSD across all radial bins that fall within the data range covered by a specific anode and energy. The resulting plots show us the distribution in the  $v_{\perp}$  versus  $v_{\parallel}$  plane and allow us to visualize both the velocity and PA distribution of the PUIs for the measured interval. Figure 4 is an example of such a plot with the black semicircle denoting the (sub)corotation velocity at the middle of the measured interval.

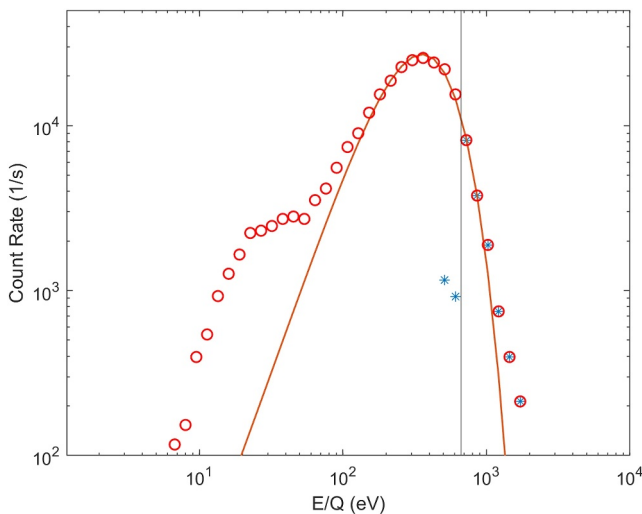


**Figure 3.** Ion counts data (red circles) with a Maxwellian distribution (orange line) fitted to it to represent the bulk ion population, for 21 November 2009 at 13:03:01 as measured by anode 4. The residuals of the subtraction are denoted by the blue stars. The subtraction was performed for ions with  $E/Q$  between the expected pick-up ion energy (black line) and the energy of corotating bulk ions. Ions below this energy are primarily protons and other lower mass species, and are not included in our analysis.

The three typical PUI distributions (ring, bispherical and accelerated) can be seen on these radial plots. Ring distributions have their maximum PSD around a single point on the semi-circle, usually at PA of 90°, representative of locally produced PUIs. Bispherical distributions, being a result of waves causing PA scattering in the ion population, are seen as high PSD around the majority of the semicircle. Accelerated ion populations have energies much

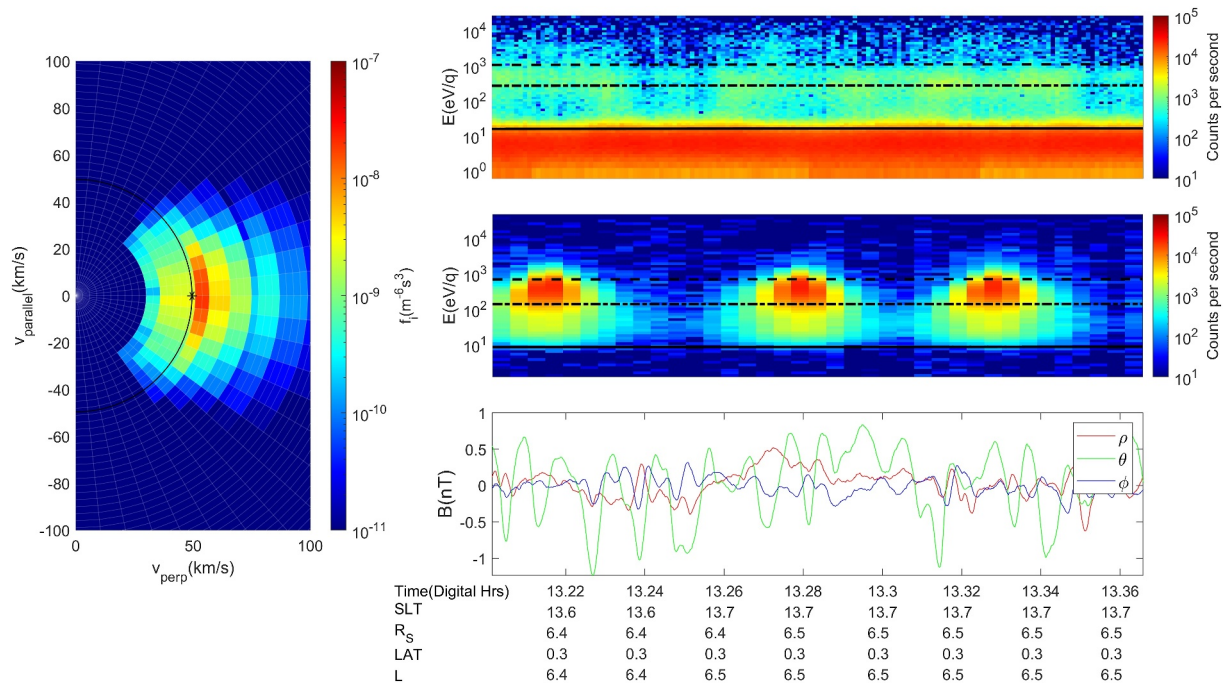


**Figure 4.** Left: the radial  $v_{\perp}$  versus  $v_{\parallel}$  plots with the black semi circle denoting the expected pick-up ion (PUI) energy and the star the location where the ring distribution is observed. Right: supplementary panels for better understanding of the data being investigated. The top and middle panels are energy per charge density plots for electrons and ions respectively. The three lines seen on the plot are reference energies for data taken at the middle of the studied interval: proton energy at corotation velocity (solid line), ion energy at corotation velocity (dashed-dotted line), PUI energy at  $v_{corot}$  (dashed line). We assume a ion mass of 16.25. The bottom panel is the magnetic field data in spherical KRTP coordinates. The data presented was gathered on 21 November 2009.

higher than the expected PUI energy so they appear as high density in areas outwards of the semi-circle.

#### 4. Results

A total of 15,211 intervals are determined to be adequate for use in our study. These intervals are used to extract the necessary information regarding the PUI distributions such as PSD, velocity and PA. We note however that due to the limited field of view of IMS the extracted distributions will not be necessarily full distributions and so the accuracy of our results will be limited. Radial PSD plots in  $v_{\perp}$  versus  $v_{\parallel}$  space are created for each 10 min interval examined throughout the investigated years. Pitch angle distributions can take several shapes, the most common ones being: pancake (Gaussian), field aligned (anti-Gaussian), butterfly (two separate peaks) and flat (no peak). We perform a check for the distribution type found in the region we investigate by plotting the average PSD at the expected PUI energy and at each PA against radial distance, averaging over all the measured intervals at a certain radial distance, as seen in Figure 5. The measured PSD is normalized to the local maximum to account for decreasing density at larger distances from the planet. For all the radial distances the distributions are overwhelmingly of the “pancake” type, centered around  $90^{\circ}$  PA.

For each radial plot made, we measure the full width at half maximum (FWHM) of the PAD and the half width at half maximum (HWHM) of the velocity distribution. The FWHM of the PA distribution is calculated at the expected PUI energy (sub-corotation velocity) at the middle of the interval. For the velocity distribution, the measurement is done at the PA where we observe the maximum density enhancement. The reason for choosing a HWHM instead of FWHM is because, even after the subtraction of the bulk population, the highest densities are usually still measured at lower velocities. We measure the HWHM starting two bins below the  $v_{corot}$  at the middle of the interval and ending at the last measured value of the distribution.

In order to compare our distribution to the incidence and strength of ICWs, we use the data processed by Long et al. (2022). Their study does not extend past seven  $R_s$ , with data taken every 2 min from 14 May 2004–31 December 2016. They use the following criteria for identifying ICWs.

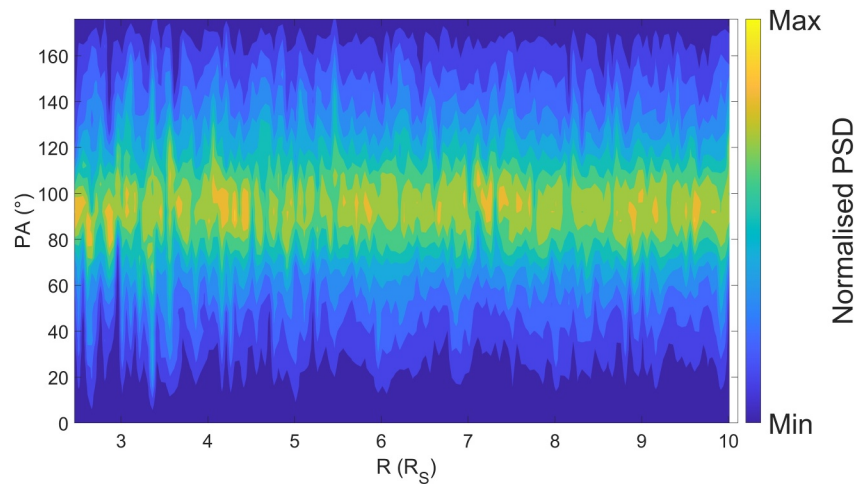


**Figure 5.** Distribution of phase space density (PSD) with respect to pitch angle and radial distance for the year 2007. PSD is normalized to the maximum local value.

- The peak frequency of the waves must be between half and twice the equatorial  $W^+$  cyclotron frequency, a criterion used by Meeks et al. (2016) and Meeks and Simon (2017).
- Each wave event must last at least 5 min, with every sample covering 10 frequency channels.

The data is plotted on the same grid as the PA and velocity distributions with the ICW amplitude being averaged for each individual bin.

The results for each type of distribution are represented in Figure 6, which comprises two global plots of the Saturnian magnetosphere for each type of distribution. Figures 6a, 6c, and 6e are top-down views of the Saturnian magnetosphere where the data is distributed into  $0.2 R_S$  by  $2.5^\circ$  bins, b,d,f are side views of magnetosphere at all local times with  $0.2 R_S$  by  $2^\circ$  bins. We also make local time versus L-shell plots, but no qualitative differences are observed when compared to the radial distance equivalents. A quality factor (Q-factor) is used to determine the trustworthiness of data from an interval. This Q-factor is the average change in spacecraft attitude (yaw, pitch and roll), with values ranging from 0 when Cassini performed no rotations on any of its axes, to 1 where there were  $360^\circ$  rotations on all three axes. A value of 0.2 is determined as the maximum acceptable Q-factor for a measurement to be considered. The use of this Q-factor is important as throughout the mission, Cassini would have periods of significant attitude change such as during scanning runs of Saturn and the moons. Hence, we determined that removing data obtained during these periods was necessary to ensure data was obtained in a consistent manner. We also note that actuator action was not taken into account as the actuator's role was to ensure a wider field of view for the instrument and so it was essential for getting accurate plasma measurements.

In Figures 6a and 6b we can see the PA distributions tend to broaden with increasing latitude, with areas around the equator having distribution widths of only a couple of tens of degrees, while at latitudes higher than  $20^\circ$  the widths reach over  $100^\circ$  in PA and forming a “Pacman”-like signature. We can be sure that this result is statistically significant as roughly two thirds of the measured intervals were measured in the equatorial region, with the remaining third being at higher latitudes of over  $10^\circ$ . ICWs on the other hand are strongest in the region around the equator (Figures 6e and 6f) where the density of plasma is highest. One exception to this are a few high amplitude bins at higher latitude in the northern hemisphere at roughly  $6 R_S$ . Long et al. (2022) cut off this part of their data and the significant departure from the rest of the data suggests these are anomalous readings rather than being physical. If we ignore these readings, the higher amplitude of ICWs doesn't lead to more PA scattering as would be expected. We show intervals in gray in Figure 6f when measurements were performed but no waves detected. This shows that most ICWs are created at around  $5^\circ$  from the equator in accordance to the M-like signature previously reported in literature (Chou & Cheng, 2017; Leisner et al., 2011; Long et al., 2022; Meeks et al., 2016; Meeks & Simon, 2017). Ion cyclotron waves are also more prevalent in the inner magnetosphere and their presence at higher latitudes is mostly limited to inside the orbit of Dione. As PUIs are the primary producers of ICWs, these observations can be confirmed by looking at the PUI density in Figure 7. The highest densities of PUIs are found around the equator and drop sharply past the orbit of Rhea. The difference between the signals

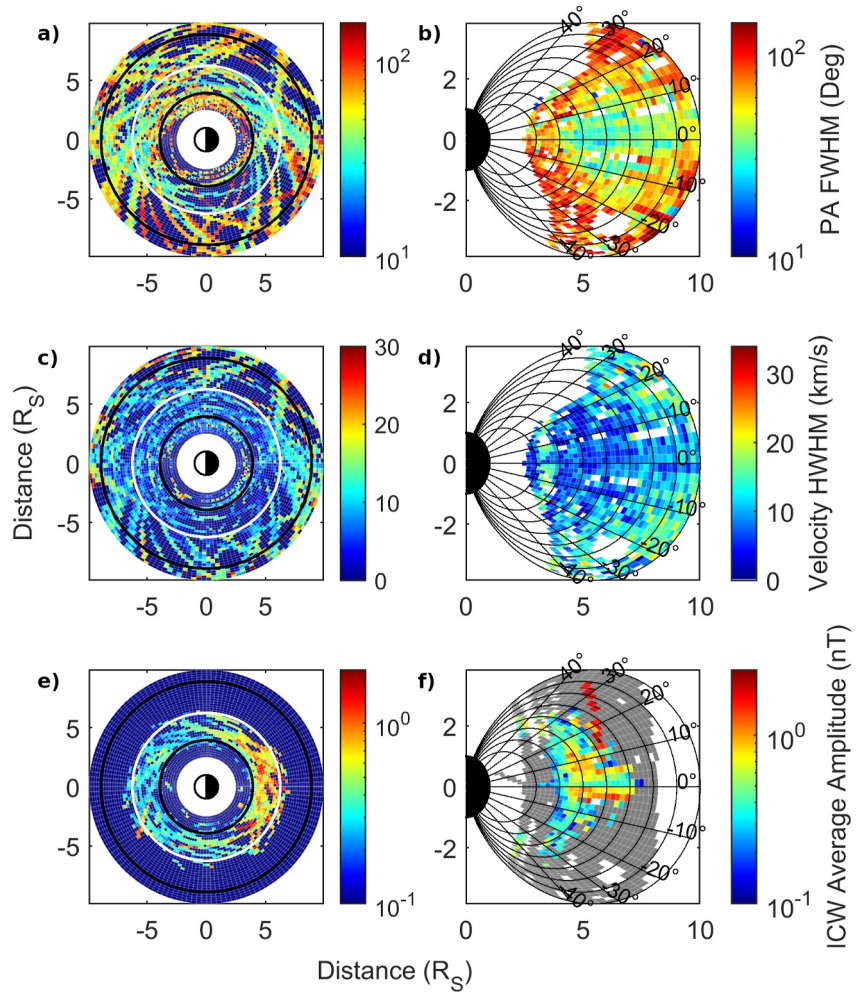


**Figure 6.** Global maps of the Saturn magnetosphere with top-down (left) and side (right) views. (a)–(b) show the pitch angle distributions shown as the full width at half maximum of the distribution at the injection velocity at the middle of the measured interval. (c)–(d) show the velocity distributions shown as half width at half maximum of the distribution. (e)–(f) show the average amplitude of ion cyclotron waves (reproduced from Long et al. (2022)). The gray bins in (f) are bins where measurements were made, but no waves were detected. In the top down view, the inner black circle is the orbit of Enceladus, the white circle is the orbit of Dione and the outer black circle is the orbit of Rhea.

seen at noon (left-hand side) and midnight (right-hand side) in the top-down view of the ICW amplitudes marks a noticeable day-night asymmetry. This same asymmetry was discussed by Long et al. (2022), who suggest that the waves are driven by ion density and velocity day-night asymmetries, leading to a similar pattern being observed in the wave amplitudes. The velocity distributions of Figures 6c and 6d show significantly less acceleration past the expected PUI velocity inside the orbit of Rhea. Past this orbit, velocity distributions suddenly increase in width by up to three times at all latitudes.

An additional check for the PA distributions can be done by looking at the anisotropy, or the measure of how far the distributions are from isotropy. According to M. W. Chen et al. (1998) and Wang et al. (2013), we can define anisotropy as:

$$A = \frac{\int_0^{\pi/2} f(\alpha_0) \sin^3 \alpha_0 d\alpha_0}{2 \int_0^{\pi/2} f(\alpha_0) \cos^2 \alpha_0 \sin \alpha_0 d\alpha_0} - 1 \quad (1)$$

where  $f$  is the measured PSD and  $\alpha_0$  is the equatorial PA.  $A = 0$  denotes isotropy, while positive and negative values represent increasing degrees of anisotropy toward “pancake” and field aligned distributions respectively.

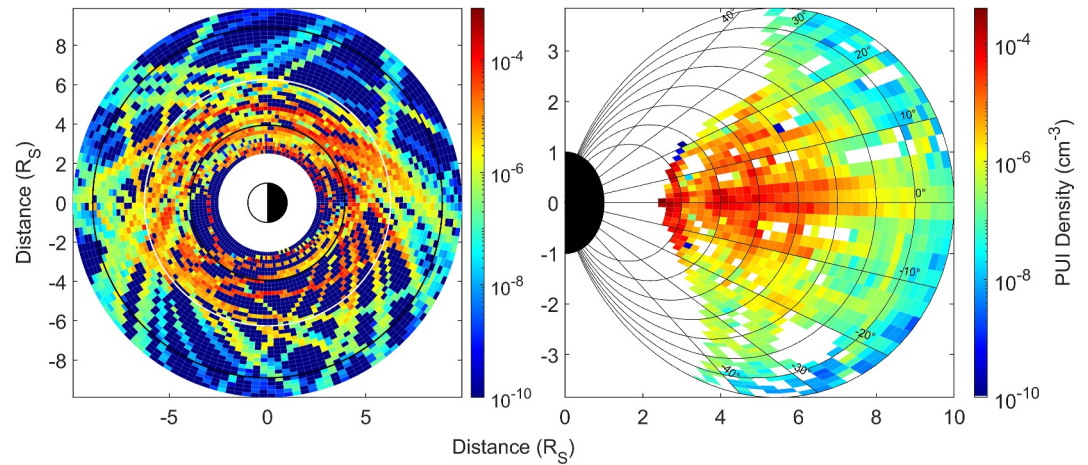


**Figure 7.** Global maps of the pick-up ion density with top-down view (left) and side view (right).

This follows from comparing the perpendicular and parallel temperatures of the ions within the distribution (e.g., Kennel and Petschek (1966)). To arrive at the exact form of Equation 1, we take the second order velocity moments in the perpendicular and parallel directions and perform a coordinate transform to achieve  $\alpha_0$  dependence. When calculated for our data, we obtain the map presented in Figure 8. This is a similar result to that presented in Figures 6a and 6b, with higher anisotropy at the equator and more isotropy at higher latitudes. We also note that all of the distributions have positive  $A$  values, which is consistent with the picture presented in Figure 5.

### 5. Discussion

The results presented in the previous section show an approximate anti-correlation between the ICW and PA distributions, with the PA distributions being widest at latitudes higher than  $10^\circ$ , while ICW amplitude peaks at  $5^\circ$  with lower amplitudes everywhere else or even no ICW presence at all.

The primary driving factor for PA scattering of PUIs is cyclotron resonance. This involves PUIs and ICWs interacting and exchanging energy which then leads to new ICW creation or PA/velocity diffusion of the ions. For ions to participate in this interaction the resonance condition must be met:

$$\omega - kv_r = \Omega_i \tag{2}$$

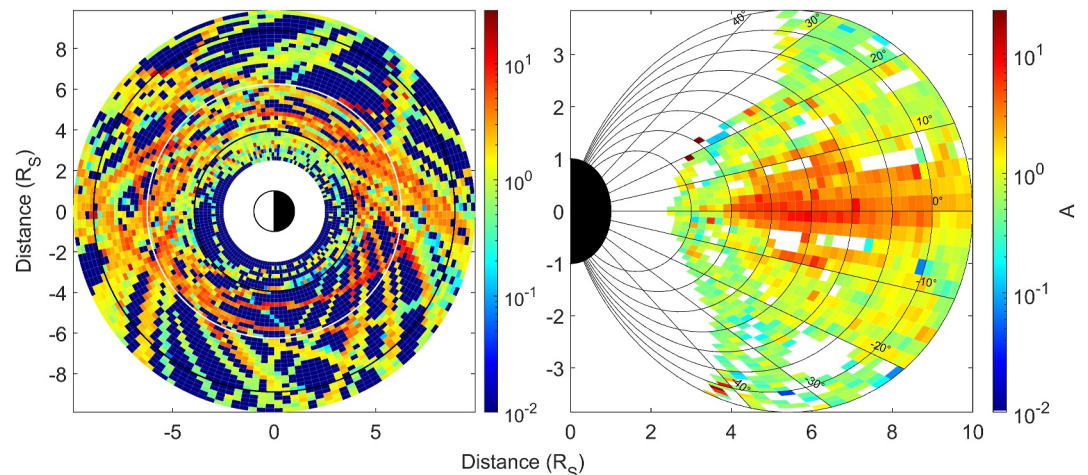


**Figure 8.** Global map of pitch angle anisotropy with top-down view (left) and side view (right).

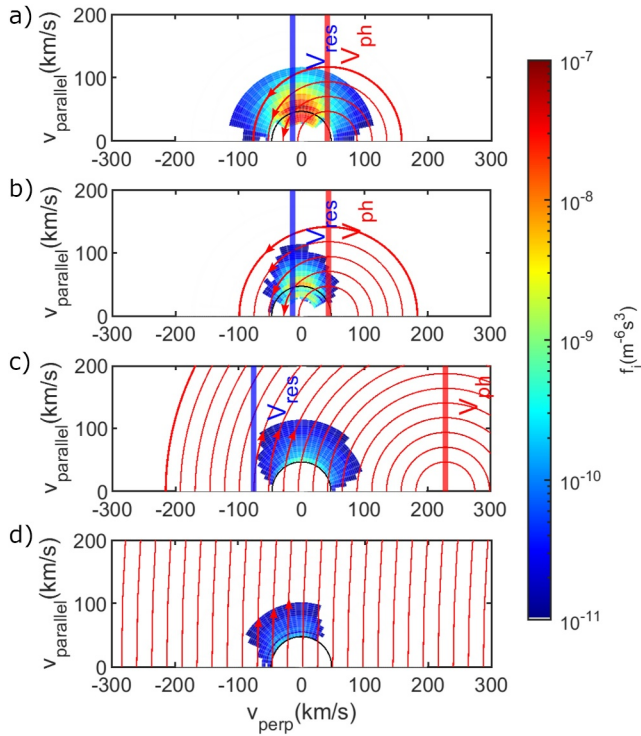


**Figure 9.** Cyclotron resonance examples in different regions of the Saturnian magnetosphere. Diffusion contours (red semicircles) are superimposed onto pick-up ion distributions for 10 min intervals. (a) 20 February 2011,  $R = 5.2 R_S$ ,  $\text{Lat} = -0.34^\circ$ ; (b) 24 July 2010,  $R = 5.2 R_S$ ,  $\text{Lat} = -3^\circ$ ; (c) 11 June 2007,  $R = 5.1 R_S$ ,  $\text{Lat} = 15.5^\circ$ ; (d) 09 September 2006,  $R = 4.15 R_S$ ,  $\text{Lat} = -24.4^\circ$ . Blue and red vertical lines show the resonant and phase velocities, respectively. Arrows indicate the direction of quasi-linear diffusion of resonant particles.  $R$  is radial distance and  $\text{Lat}$  is latitude.

where  $\omega$  is the resonant frequency,  $v_r$  is the resonant velocity,  $k$  is the wavenumber and  $\Omega_i$  is the ion cyclotron frequency. From here we can use quasi-linear theory to determine the resonant and phase velocities. Following Dusenbery and Hollweg (1981) and Isenberg (1984) we write the resonant and phase velocities as:

$$v_r = \frac{\omega}{k} \left( 1 - \frac{\Omega_i}{\omega} \right) \quad (3)$$

$$\frac{\omega}{k} = V_A \left( 1 - \frac{\omega}{\Omega_i} \right)^{\frac{1}{2}} \quad (4)$$

where  $V_A$  is the Alfvén speed.

Ions with velocities comparable to the resonant velocity exchange energy with the waves and the distribution becomes either more or less isotropic. Figure 9 illustrates how particles at velocities comparable to  $v_r$  resonate with waves of phase velocity  $\omega/k$ , which leads to quasi-linear diffusion and driving or damping of the ICWs. The minimum frequency used by studies like Meeks et al. (2016), Meeks and Simon (2017) or Long et al. (2022) is half the ion cyclotron frequency, while the maximum is twice the ion cyclotron frequency. These were chosen as the waves are created by a group of ions with similar masses rather than just one species. However, we note that resonant frequencies higher than the cyclotron frequency would lead to imaginary resonant velocities according to Equation 3. For these plots we therefore set our resonant frequency to  $0.75\Omega_i$  as a middle ground between the extreme cases of  $0.5\Omega_i$  and  $\Omega_i$ . By performing a frequency analysis on the magnetic field data with the background subtracted across the events documented by Long et al. (2022), we find that this is a reasonable approximation for the measured peak frequencies which are always lower than the OH cyclotron frequency. The arrows show the direction of the diffusion, which always points in the direction tangent to circles centered around  $\omega/k$  and from larger

values of the PSD toward smaller values of the PSD. In the cases where the particles' perpendicular velocity drops, energy is transferred to the waves (driving), while where the particle perpendicular velocity is increased, energy is removed from the waves (damping). Quasi-linear diffusion occurs in both velocity and PA, with PA diffusion being the primary effect when the ion velocity is lower than the maximum phase velocity (Kennel & Engelmann, 1966). Velocity diffusion dominates in the opposite case.

To better visualize the effect of cyclotron resonance on the scale of the magnetosphere, in Figure 10 we plot the difference between the expected PUI velocity (i.e., subcorotation) and the phase velocity of the waves. In this case we use a resonant frequency of  $0.5\Omega_i$  as it both serves as the lower limit of the investigated ICW frequency range and because for this particular case both the phase and resonant velocities happen to be equal in magnitude. In the equatorial region the phase velocity is within 100 Km/s of the ion velocity and past the orbit of Dione, it is below it. By comparison, at higher latitudes the phase speed increases to the point it approaches the speed of light. Because of this, for our calculations we use the speed of light as the phase speed in Equation 3 if it would otherwise exceed  $c$ . We can therefore conclude that PA scattering should be primarily an equatorial process, with velocity diffusion occurring instead at higher latitudes.

This significant difference between phase/resonance velocity at low and high latitudes can be best explained by the local Alfvén speed in those regions. According to Rusaitis et al. (2021), the typical Alfvén speed at the equator is under 100 km/s, while at high latitudes it can reach over  $10^4$  km/s. This means that at high latitudes waves move at such high velocities that they are unable to resonate with ions and leading to little to no wave growth, something also observed in the ICW amplitude and occurrence rates which are significantly lower in these regions. Ion cyclotron wave amplitude drops just inside the orbit of Enceladus which is also where we find a high PUI density. We therefore expect the PUIs to be driving waves in this region, however the very high Alfvén speed inhibits this

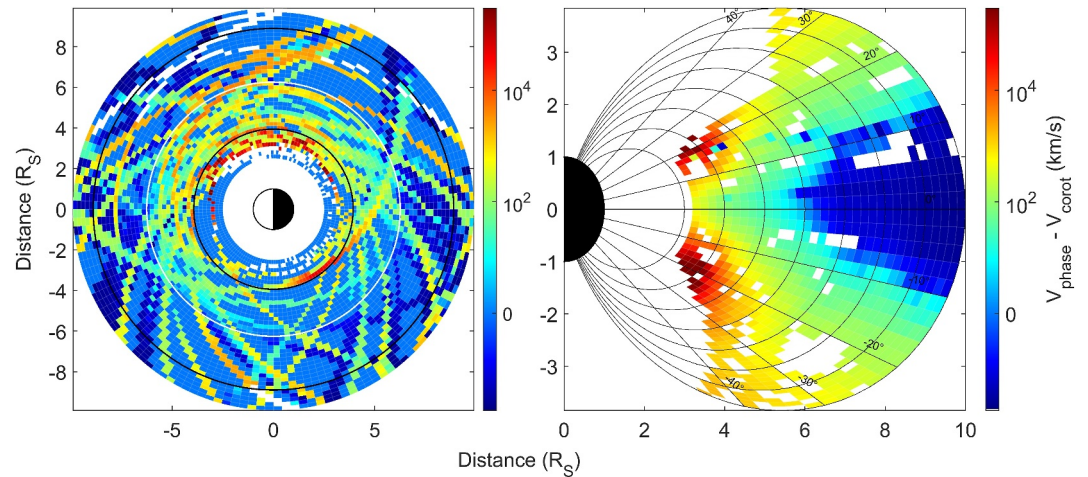


**Figure 10.** Global maps of the difference between the (sub) corotation and phase velocities.

process. The reason for the high Alfvén speed is different for each of the two cases: for the high latitude case, the Alfvén speed is increased due to a very low plasma density ( $<0.1 \text{ cm}^{-3}$ ) in those regions (see Rusaitis et al. (2021)'s Figure 1a for more information). For the case inside the orbit of Enceladus, the Alfvén speed is increased because of the very high B field of over 80 nT.

Both the presence of ICWs and the resonance condition suggest PA scattering occurs at the equator. The PA scattering time is defined as (Johnstone, 1995):

$$\tau_s^{-1} = \Omega_i \left( \frac{\delta B}{B_0} \right)^2 \quad (5)$$

where  $\tau_s$  is the PA scattering rate,  $\delta B$  is the wave amplitude and  $B_0$  is the background magnetic field. We calculated the PA scattering time for several ICW events documented by Long et al. (2022) and the results are presented in Table 1. The PA scattering time roughly follows the intensity of ICWs, with the shortest time scales being observed at around  $4 - 5^\circ$  from the equator, which is indicative of the previously reported M-like signature. This vertical variation in ICW amplitude was attributed to two potential processes. The first is convective growth of the waves, where the ICWs increase in energy by as much as an order of magnitude, while the plasma density drops rapidly. Alternatively, the increase in wave amplitude could be accompanied by a drop in wave group velocity. The lack of electric field measurements from Cassini means that the Poynting vector, which is necessary for determining the definite cause of the M-signature, cannot be calculated.

The time scale at high latitudes is two orders of magnitude higher than at the equator, confirming that little to no scattering occurs there. In Table 1 we list the bounce period  $T_B$  for the corresponding event, assuming  $\sim 90^\circ$  equatorial PA and a dipolar magnetic field. When compared to the PA scattering time, we can see that particles typically complete at least two full bounce cycles before the ions are scattered. When this is combined with the lower scattering times at high latitudes and at  $0^\circ$ , we conclude that ions have reached latitudes of over  $10^\circ$  by the time they have been significantly scattered in PA. Newly created PUIs are concentrated in the equatorial region, further skewing the observed PA distribution toward anisotropy in that region.

We now turn our attention back to our results from the previous section. Figure 10 showed that ICW production primarily happens in the equatorial region, with ICW resonance being the primary drivers of PA scattering. The presence of wider PA distributions is then explained instead by the scattering time, which is relatively long compared to the bounce period, with PUIs

**Table 1**  
*Ion Cyclotron Wave Events With Comparison Between the Pitch Angle Scattering and Bounce Time Scales*

Date	Radial distance ( $R_S$ )	Latitude (Deg)	$T_S$ (h)	$T_B$ (h)
11-Oct-05	4.50	0.03	359.64	4.79
12-Oct-06	6.15	-0.86	43.44	6.79
09-Nov-06	5.03	2.05	81.13	5.37
24-Apr-07	6.75	3.10	11.13	6.75
10-May-07	5.02	5.58	10.02	5.35
26-Jul-09	4.13	-31.45	1,621	4.33
26-Jul-09	4.62	4.10	173.11	4.61
24-Jul-10	5.50	-3.40	151.51	5.82
13-Aug-10	5.92	-3.57	4.34	6.16
10-Jan-11	4.86	-0.02	125.22	5.16

becoming fully scattered only once they have left the equator for higher latitudes. In addition to this, we note that the pattern seen in Figure 10 is very similar to that found in our PA distributions. This suggests that another contributor to our observed pattern is the higher incidence of newly created PUIs at the equator. This is because ICWs are created by the scattering of PUIs with anisotropic distributions which are more prevalent at the equator where they get picked up. Hence we expect the few highly scattered PUIs that do pass through the equatorial region as part of their bounce motion to be overshadowed by the more dominant newly injected PUIs.

The M-like signature visible in the ICW amplitude as a function of distance to the equator and described originally by Leisner et al. (2011) is not observed in our PA and velocity distributions. This is likely because the CAPS instrument has a much lower time resolutions (maximum  $\sim 4$ s) compared to the Cassini magnetometer ( $< 1$ s at full resolution). Even at lower resolutions of 1 s as used by Leisner et al. (2011) and Meeks and Simon (2017), the CAPS-IMS instrument would have a maximum resolution of 4 s and going up to 32 s. For example, during the E2 flyby of Enceladus in 2005, Cassini would have traveled 6.1 km above the equator between consecutive data points, compared to CAPS' 97.6 km (16 s resolution at the time). Meeks and Simon (2017), Chou and Cheng (2017) and Long et al. (2022) performed spectral analysis for most of the Cassini mission, and all detected the M-like signature. It is hence a possibility that the signature is not a transient phenomenon but rather a persistent one. Alternatively, the limited field of view of IMS could be impacting the visibility of the M-like signature. Therefore, with IMS not viewing the entire plasma population and with no forward modeling to replace missing data, this could also be a cause of the lack of an M-like signature in our ion data.

## 6. Summary and Conclusions

In this paper we set out to examine the distribution of PUIs in the extended neutral cloud from thermal ion data obtained by the Cassini CAPS instrument. This investigation allows us to develop a better understanding of how PUIs are distributed in the magnetosphere of Saturn, and to explain what effects wave particle interactions have on the distribution and dynamics of PUIs. In order to achieve this goal, we analyzed data from the CAPS instrument for the majority of its lifetime (2005–2012) for when the Cassini spacecraft was within  $10R_S$  of Saturn, an area which roughly corresponds to the densest part of the extended neutral cloud. The data from the IMS component of CAPS is processed by subtracting the background and penetrating radiation as well as the core ion population. The resulting data is then plotted onto  $v_{\perp}$  versus  $v_{\parallel}$  plots from which the PA and velocity distributions are then extracted. The obtained distributions are then put into bins on global maps of the examined region. Two patterns can be observed on these distribution maps.

1. The PA distributions broaden with increasing latitude, with the widest distributions found past  $10^{\circ}$ . This resulting “Pacman”-like signature, extending from the orbit of Enceladus to the orbit of Rhea, is found to be roughly anti-correlated with the distribution of ICWs with latitude (Long et al., 2022). The explanation for this is the relatively slow PA scattering time compared to the PUI bounce period, leading to ions getting highly scattered only once they have reached higher latitudes. We also expect the higher incidence of newly created PUIs in the equatorial region to contribute to the observed distributions.
2. The velocity distributions show that inside the orbit of Rhea there is little acceleration of the ions, with velocity distribution HWHM extending only up to around 10 km/s on average compared to the velocity of the bulk plasma (Wilson et al., 2008). Past Rhea however we see that distributions broaden significantly, likely as a result of increases in plasma temperature and reductions in plasma density leading to energy being distributed over fewer particles.

The work done in this paper serves as another piece of the puzzle of the Saturnian magnetosphere. Thomsen et al. (2010) gave us a large scale description of the Saturnian system by investigating thermal ion parameters for the majority of Saturn's magnetosphere ( $3 - 30R_S$ ), but without making a distinction between PUIs and the Maxwellian core distribution. Sittler et al. (2004), Tokar et al. (2008), Teolis et al. (2010) and Desai et al. (2017) furthered our understanding of PUI distribution in density, composition, PA and velocity, focusing on the local environments of the icy moons visited by Cassini. Ion cyclotron waves were extensively studied in the inner magnetosphere (e.g., Leisner et al., 2011). Meanwhile, at Titan pick-up and sporadic ICW activity (Regoli et al., 2016; Russell et al., 2016) has been previously reported, but with much lower incidence as explained by Cowee et al. (2010). Our paper complements the picture already provided by these various studies. It expands upon the work of Thomsen et al. (2010) and the icy moon studies by providing PA and velocity distributions from inside the orbit of Enceladus to just beyond the orbit of Rhea, as well as covering higher latitudes.

## Data Availability Statement

The data supporting this work can be obtained from <https://doi.org/10.5281/zenodo.10805240> (Radulescu et al., 2024).

## Acknowledgments

CRR acknowledges support from the Science and Technology Facilities Council (STFC) studentship ST/W507891 and for Long Term Attachment support from STFC; AJC, GHJ and DV acknowledge partial support from STFC grant ST/W001004/1. CRR is grateful for the hospitality provided at Georgia Tech where this study was completed.

## References

- Arridge, C., André, N., McAndrews, H., Bunce, E., Burger, M., Hansen, K., et al. (2011). Mapping magnetospheric equatorial regions at saturn from cassini prime mission observations. *Space Science Reviews*, *164*(1–4), 1–83. <https://doi.org/10.1007/s11214-011-9850-4>
- Bagenal, F., & Delamere, P. A. (2011). Flow of mass and energy in the magnetospheres of jupiter and saturn. *Journal of Geophysical Research*, *116*(A5). Retrieved from <https://doi.org/10.1029/2010JA016294>
- Brace, L. H., Kasprzak, W. T., Taylor, H. A., Theis, R. F., Russell, C. T., Barnes, A., et al. (1987). The iontail of venus: Its configuration and evidence for ion escape. *Journal of Geophysical Research*, *92*(A1), 15–26. Retrieved from <https://doi.org/10.1029/JA092iA01p00015>
- Cassidy, T. A., & Johnson, R. E. (2010). Collisional spreading of Enceladus' neutral cloud. *Icarus*, *209*(2), 696–703. <https://doi.org/10.1016/j.icarus.2010.04.010>
- Chen, M. W., Roeder, J. L., Fennell, J. F., Lyons, L. R., & Schulz, M. (1998). Simulations of ring current proton pitch angle distributions. *Journal of Geophysical Research*, *103*(A1), 165–178. Retrieved from <https://agupubs.onlinelibrary.wiley.com/doi/abs/10.1029/97JA02633>
- Chen, Y., Hill, T. W., Rymer, A. M., & Wilson, R. J. (2010). Rate of radial transport of plasma in saturn's inner magnetosphere. *Journal of Geophysical Research*, *115*(A10). Retrieved from <https://agupubs.onlinelibrary.wiley.com/doi/abs/10.1029/2010JA015412>
- Chou, M., & Cheng, C. Z. (2017). Distribution of water-group ion cyclotron waves in Saturn's magnetosphere. *Earth Planets and Space*, *69*(1), 122. <https://doi.org/10.1186/s40623-017-0709-0>
- Coates, A. J. (2010). Ion pickup at comets: Comparison with other unmagnetized objects. In J. Le Roux, G. P. Zank, A. J. Coates, & V. Florinski (Eds.), *Pickup ions throughout the heliosphere and beyond* (Vol. 1302, pp. 213–224). <https://doi.org/10.1063/1.3529973>. AIP Conference Proceedings
- Coates, A. J. (2012). Ion pickup and acceleration: Measurements from planetary missions. In J. Heerikhuisen, G. Li, N. Pogorelov, & G. Zank (Eds.), *Physics of the heliosphere: A 10 year retrospective* (Vol. 1436, pp. 89–102). <https://doi.org/10.1063/1.4723595>. AIP Conference Proceedings
- Coates, A. J. (2017). Pickup particle acceleration at comets, moons and magnetospheres. *Journal of Physics: Conference Series*, *900*, 012002. <https://doi.org/10.1088/1742-6596/900/1/012002>
- Coates, A. J., Johnstone, A. D., Kessel, R. L., Huddleston, D. E., Wilken, B., Jockers, K., & Neubauer, F. M. (1990a). Plasma parameters near the comet Halley bow shock. *Journal of Geophysical Research*, *95*(A12), 20701–20716. Retrieved from <https://agupubs.onlinelibrary.wiley.com/doi/abs/10.1029/JA095iA12p20701>
- Coates, A. J., Johnstone, A. D., Wilken, B., Jockers, K., & Glassmeier, K.-H. (1989). Velocity space diffusion of pickup ions from the water group at comet Halley. *Journal of Geophysical Research*, *94*(A8), 9983–9993. Retrieved from <https://agupubs.onlinelibrary.wiley.com/doi/abs/10.1029/JA094iA08p09983>
- Coates, A. J., Johnstone, A. D., Wilken, B., & Neubauer, F. M. (1993). Velocity space diffusion and nongyrotropy of pickup water group ions at comet grigg-skjellerup. *Journal of Geophysical Research*, *98*(A12), 20985–20994. Retrieved from <https://agupubs.onlinelibrary.wiley.com/doi/abs/10.1029/93JA02535>
- Coates, A. J., Wilken, B., Johnstone, A. D., Jockers, K., Glassmeier, K.-H., & Huddleston, D. E. (1990b). Bulk properties and velocity distributions of water group ions at comet Halley: Giotto measurements. *Journal of Geophysical Research*, *95*(A7), 10249–10260. Retrieved from <https://agupubs.onlinelibrary.wiley.com/doi/abs/10.1029/JA095iA07p10249>
- Cowee, M. M., Gary, S. P., Wei, H. Y., Tokar, R. L., & Russell, C. T. (2010). An explanation for the lack of ion cyclotron wave generation by pickup ions at titan: 1-d hybrid simulation results. *Journal of Geophysical Research*, *115*(A10). Retrieved from <https://doi.org/10.1029/2010JA015769>
- Desai, R. T., Cowee, M. M., Wei, H., Fu, X., Gary, S. P., Volwerk, M., & Coates, A. J. (2017). Hybrid simulations of positively and negatively charged pickup ions and cyclotron wave generation at europa. *Journal of Geophysical Research: Space Physics*, *122*(10), 10408–10420. Retrieved from <https://doi.org/10.1002/2017JA024479>
- Desai, R. T., Taylor, S. A., Regoli, L. H., Coates, A. J., Nordheim, T. A., Cordiner, M. A., et al. (2018). Cassini caps identification of pickup ion compositions at reha. *Geophysical Research Letters*, *45*(4), 1704–1712. Retrieved from <https://doi.org/10.1002/2017GL076588>
- Dougherty, M. K., Kellock, S., Southwood, D., Balogh, A., Smith, E., Tsurutani, B., et al. (2004). The cassini magnetic field investigation. *Space Science Reviews*, *114*(1–4), 331–383. <https://doi.org/10.1007/s11214-004-1432-2>
- Dougherty, M. K., Khurana, K. K., Neubauer, F. M., Russel, C. T., Saur, J., Leisner, J. S., & Burton, M. E. (2006). Identification of a dynamic atmosphere at enceladus with the cassini magnetometer. *Science*, *311*(5766), 1406–1409. Retrieved from <https://doi.org/10.1126/science.1120985>
- Dusenbery, P. B., & Hollweg, J. V. (1981). Ion-cyclotron heating and acceleration of solar wind minor ions. *Journal of Geophysical Research*, *86*(A1), 153–164. Retrieved from <https://agupubs.onlinelibrary.wiley.com/doi/abs/10.1029/JA086iA01p00153>
- Fleshman, B. L., Delamere, P. A., & Bagenal, F. (2010). Modeling the enceladus plume–plasma interaction. *Geophysical Research Letters*, *37*(3). Retrieved from <https://doi.org/10.1029/2009GL041613>
- Gloeckler, G., Hovestadt, D., Ipavich, F. M., Scholer, M., Klecker, B., & Galvin, A. B. (1986). Cometary pick-up ions observed near Giacobini-Zinner. *Geophysical Research Letters*, *13*(3), 251–254. <https://doi.org/10.1029/GL013i003p00251>
- Hartle, R. E., Sittler, E. C., Jr., Neubauer, F. M., Johnson, R. E., Smith, H. T., Cray, F., et al. (2006). Preliminary interpretation of titan plasma interaction as observed by the cassini plasma spectrometer: Comparisons with voyager 1. *Geophysical Research Letters*, *33*(8). Retrieved from <https://doi.org/10.1029/2005GL024817>
- Isenberg, P. A. (1984). Resonant acceleration and heating of solar wind ions: Anisotropy and dispersion. *Journal of Geophysical Research*, *89*(A8), 6613–6622. Retrieved from <https://agupubs.onlinelibrary.wiley.com/doi/abs/10.1029/JA089iA08p06613>
- Johnson, R. E., Smith, H. T., Tucker, O. J., Liu, M., Burger, M. H., Sittler, E. C., & Tokar, R. L. (2006). The enceladus and OH tori at saturn. *The Astrophysical Journal*, *644*(2), L137–L139. <https://doi.org/10.1086/505750>
- Johnstone, A. (1995). Cometary ion pickup processes: Halley and grigg-skjellerup compared. *Advances in Space Research*, *16*(4), 11–18. (Comparative Studies of Magnetospheric Phenomena) Retrieved from [https://doi.org/10.1016/0273-1177\(95\)00202-P](https://doi.org/10.1016/0273-1177(95)00202-P)
- Jurac, S., & Richardson, J. D. (2005). A self-consistent model of plasma and neutrals at saturn: Neutral cloud morphology. *Journal of Geophysical Research*, *110*(A9). Retrieved from <https://doi.org/10.1029/2004JA010635>

- Kallenbach, R., Geiss, J., Gloeckler, G., & von Steiger, R. (2000). Pick-up ion measurements in the heliosphere - a review. *Astrophysics and Space Science*, 274, 97–114. <https://doi.org/10.1023/A:1026587620772>
- Keckskemety, K., & Cravens, T. E. (1993). Pick-up ions at pluto. *Geophysical Research Letters*, 20(7), 543–546. <https://doi.org/10.1029/93GL00487>
- Kennel, C. F., & Engelmann, F. (1966). Velocity space diffusion from weak plasma turbulence in a magnetic field. *Physics of Fluids*, 9(12), 2377–2388. <https://doi.org/10.1063/1.1761629>
- Kennel, C. F., & Petschek, H. E. (1966). Limit on stably trapped particle fluxes. *Journal of Geophysical Research (1896-1977)*, 71(1), 1–28. Retrieved from <https://agupubs.onlinelibrary.wiley.com/doi/abs/10.1029/JZ071i001p00001>
- Leisner, J. S., Russell, C. T., Dougherty, M. K., Blanco-Cano, X., Strangeway, R. J., & Bertucci, C. (2006). Ion cyclotron waves in saturn's e ring: Initial cassini observations. *Geophysical Research Letters*, 33(11). Retrieved from <https://doi.org/10.1029/2005GL024875>
- Leisner, J. S., Russell, C. T., Wei, H. Y., & Dougherty, M. K. (2011). Probing Saturn's ion cyclotron waves on high-inclination orbits: Lessons for wave generation. *Journal of Geophysical Research (Space Physics)*, 116(A9), A09235. <https://doi.org/10.1029/2011JA016555>
- Long, M., Cao, X., Gu, X., Ni, B., Qu, S., Ye, S., et al. (2022). Statistics of water-group band ion cyclotron waves in saturn's inner magnetosphere based on 13 yr of cassini measurements. *The Astrophysical Journal*, 932(1), 56. <https://doi.org/10.3847/1538-4357/ac6bf0>
- Mall, U., Kirsch, E., Cierpka, K., Wilken, B., Söding, A., Neubauer, F., et al. (1998). Direct observation of lunar pick-up ions near the Moon. *Geophysical Research Letters*, 25(20), 3799–3802. <https://doi.org/10.1029/1998GL900003>
- Meeks, Z., & Simon, S. (2017). Magnetic signatures of ion cyclotron waves during cassini's high-inclination orbits of saturn. *Planetary and Space Science*, 136, 34–45. Retrieved from <https://doi.org/10.1016/j.pss.2016.12.006>
- Meeks, Z., Simon, S., & Kabanovic, S. (2016). A comprehensive analysis of ion cyclotron waves in the equatorial magnetosphere of saturn. *Planetary and Space Science*, 129, 47–60. Retrieved from <https://doi.org/10.1016/j.pss.2016.06.003>
- Nordheim, T. A., Wellbrock, A., Jones, G. H., Desai, R. T., Coates, A. J., Teolis, B. D., & Jasinski, J. M. (2020). Detection of negative pickup ions at saturn's moon dione. *Geophysical Research Letters*, 47(7), e2020GL087543. Retrieved from <https://doi.org/10.1029/2020GL087543>
- Poppe, A. R., Halekas, J. S., Szalay, J. R., Horányi, M., Levin, Z., & Kempf, S. (2016). Ladee/idx observations of lunar pickup ion distribution and variability. *Geophysical Research Letters*, 43(7), 3069–3077. Retrieved from <https://doi.org/10.1002/2016GL068393>
- Porco, C. C., Helfenstein, P., Thomas, P. C., Ingersoll, A. P., Wisdom, J., West, R., et al. (2006). Cassini observes the active south Pole of enceladus. *Science*, 311(5766), 1393–1401. <https://doi.org/10.1126/science.1123013>
- Radulescu, C. R., Coates, A. J., Simon, S., & Jones, G. H. (2024). Data for "Pick-up ion distributions in the inner and middle Saturnian Magnetosphere" by Radulescu et al., Vol. 2024. Zenodo. [Dataset]. <https://doi.org/10.5281/zenodo.10805240>
- Regoli, L. H., Coates, A. J., Thomsen, M. F., Jones, G. H., Roussos, E., Waite, J. H., et al. (2016). Survey of pickup ion signatures in the vicinity of titan using caps/ims. *Journal of Geophysical Research: Space Physics*, 121(9), 8317–8328. Retrieved from <https://doi.org/10.1002/2016JA022617>
- Rusaitis, L., Khurana, K. K., Kivelson, M. G., & Walker, R. J. (2021). Quasiperiodic 1-hour alfvén wave resonances in saturn's magnetosphere: Theory for a realistic plasma/field model. *Geophysical Research Letters*, 48(7), e2020GL090967. Retrieved from <https://doi.org/10.1029/2020GL090967>
- Russell, C. T., Wei, H. Y., Cowee, M. M., Neubauer, F. M., & Dougherty, M. K. (2016). Ion cyclotron waves at titan. *Journal of Geophysical Research: Space Physics*, 121(3), 2095–2103. Retrieved from <https://doi.org/10.1002/2015JA022293>
- Santolik, O., Gurnett, D. A., Jones, G. H., Schippers, P., Cray, F. J., Leisner, J. S., et al. (2011). Intense plasma wave emissions associated with saturn's moon rhea. *Geophysical Research Letters*, 38(19). Retrieved from <https://doi.org/10.1029/2011GL049219>
- Sittler, E., Andre, N., Blanc, M., Burger, M., Johnson, R., Coates, A., et al. (2008). Ion and neutral sources and sinks within saturn's inner magnetosphere: Cassini results. *Planetary and Space Science*, 56(1), 3–18. (Surfaces and Atmospheres of the Outer Planets, their Satellites and Ring Systems: Part III) Retrieved from <https://doi.org/10.1016/j.pss.2007.06.006>
- Sittler, E. C., Johnson, R. E., Jurac, S., Richardson, J. D., McGrath, M., Cray, F., et al. (2004). Pickup ions at dione and enceladus: Cassini plasma spectrometer simulations. *Journal of Geophysical Research*, 109(A1). Retrieved from <https://doi.org/10.1029/2002JA009647>
- Sittler, E. C., Johnson, R. E., Richardson, J. D., Jurac, S., McGrath, M. A., & Young, D. (2000). Pickup ions at dione and enceladus. *EOS Transactions*, 81, 48.
- Smith, H. T., Johnson, R. E., Perry, M. E., Mitchell, D. G., McNutt, R. L., & Young, D. T. (2010). Enceladus plume variability and the neutral gas densities in saturn's magnetosphere. *Journal of Geophysical Research*, 115(A10). Retrieved from <https://agupubs.onlinelibrary.wiley.com/doi/abs/10.1029/2009JA015184>
- Teolis, B. D., Jones, G. H., Miles, P. F., Tokar, R. L., Magee, B. A., Waite, J. H., et al. (2010). Cassini finds an oxygen-carbon dioxide atmosphere at saturn's icy moon rhea. *Science*, 330(6012), 1813–1815. Retrieved from <https://doi.org/10.1126/science.1198366>
- Thomsen, M. F., Reisenfeld, D. B., Delapp, D. M., Tokar, R. L., Young, D. T., Cray, F. J., et al. (2010). Survey of ion plasma parameters in saturn's magnetosphere. *Journal of Geophysical Research*, 115(A10). Retrieved from <https://agupubs.onlinelibrary.wiley.com/doi/abs/10.1029/2010JA015267>
- Tokar, R. L., Johnson, R. E., Hill, T. W., Pontius, D. H., Kurth, W. S., Cray, F. J., et al. (2006). The interaction of the atmosphere of enceladus with saturn's plasma. *Science*, 311(5766), 1409–1412. Retrieved from <https://doi.org/10.1126/science.1121061>
- Tokar, R. L., Johnson, R. E., Thomsen, M. F., Sittler, E. C., Coates, A. J., Wilson, R. J., et al. (2012). Detection of exospheric o<sub>2</sub><sup>+</sup> at saturn's moon dione. *Geophysical Research Letters*, 39(3). Retrieved from <https://doi.org/10.1029/2011GL050452>
- Tokar, R. L., Wilson, R., Johnson, R., Henderson, M., Thomsen, M., Cowee, M., et al. (2008). Cassini detection of water-group pick-up ions in the enceladus torus. *Geophysical Research Letters*, 35(14). <https://doi.org/10.1029/2008GL034749>
- Wang, C.-P., Zaharia, S. G., Lyons, L. R., & Angelopoulos, V. (2013). Spatial distributions of ion pitch angle anisotropy in the near-earth magnetosphere and tail plasma sheet. *Journal of Geophysical Research: Space Physics*, 118(1), 244–255. Retrieved from <https://doi.org/10.1029/2012JA018275>
- Wilson, R. J., Tokar, R. L., & Henderson, M. G. (2009). Thermal ion flow in saturn's inner magnetosphere measured by the cassini plasma spectrometer: A signature of the enceladus torus? *Geophysical Research Letters*, 36(23). Retrieved from <https://doi.org/10.1029/2009GL040225>
- Wilson, R. J., Tokar, R. L., Henderson, M. G., Hill, T. W., Thomsen, M. F., & Pontius, D. H., Jr. (2008). Cassini plasma spectrometer thermal ion measurements in saturn's inner magnetosphere. *Journal of Geophysical Research*, 113(A12). Retrieved from <https://agupubs.onlinelibrary.wiley.com/doi/abs/10.1029/2008JA013486>
- Young, D. T., Berthelier, J.-J., Blanc, M., Burch, J., Coates, A., Grande, M., et al. (2004). Cassini plasma spectrometer investigation. *Space Science Reviews*, 114(1–4), 1–112. <https://doi.org/10.1007/s11214-004-1406-4>
- Young, D. T., Berthelier, J.-J., Blanc, M., Burch, J. L., Bolton, S., Coates, A. J., et al. (2005). Composition and dynamics of plasma in saturn's magnetosphere. *Science*, 307(5713), 1262–1266. Retrieved from <https://doi.org/10.1126/science.1106151>